PERGAMON

Journal of Structural Geology 24 (2002) 1845–1856

JOURNAL OF STRUCTURAL GEOLOGY

www.elsevier.com/locate/jstrugeo

Cataclastic deformation of garnet: a record of synseismic loading and postseismic creep

Claudia A. Trepmann*, Bernhard Stöckhert[1]

Endogene Geologie, Institut für Geologie, Mineralogie und Geophysik, Ruhr-Universität Bochum, D-44780 Bochum, Germany

Received 24 July 2001; revised 18 December 2001; accepted 18 December 2001

Abstract

Microstructural evidence for episodic deformation of the uppermost plastosphere related to failure of the schizosphere in major seismic events has been previously reported from the Sesia Zone, Western Alps, with inferred extraordinarily high stresses and strain rates for the early stages of creep during stress relaxation at temperatures of about 300–350 °C. In some of these rocks, crystals of the high strength mineral garnet embedded in a quartz matrix are intensely fragmented. Detailed optical, electron microprobe and scanning electron microscopic study, combined with electron backscatter diffraction techniques, suggests that fragmentation of garnet took place quasi-instantaneously at very high peak stresses. Subsequent deformation during stress relaxation caused displacement of the garnet fragments by frictional sliding, controlled by dislocation creep in the surrounding quartz matrix. In a final stage, after restoration of a near-lithostatic pore fluid pressure, the garnet fragments were pulled apart and the opening cracks were filled by quartz and feldspar precipitated from the pore fluid. This record appears to be consistent with the proposed model of synseismic loading and postseismic creep, and the related pore pressure changes.

Keywords: Garnet; Deformation; Microstructure

1. Introduction

The mechanical behavior of rocks in the upper crust is generally governed by primarily pressure-dependent frictional behavior, giving way to primarily temperature-dependent plastic flow at greater depth (e.g. Goetze and Evans, 1979; Brace and Kohlstedt, 1980; Sibson, 1980; Scholz, 1990; Evans and Kohlstedt, 1995; Kohlstedt et al., 1995). Whereas the lower crust deforms slowly by dislocation creep or diffusion creep of its major mineralogical constituents, with strain rates on the order of 10^{-14} to $10^{-16}\,s^{-1}$, deformation in the brittle upper crust can take place by sudden displacement along faults during earthquakes (e.g. Yeats et al., 1997). Scholz (1990) proposed the term schizosphere for the brittle seismogenic upper layer and the term plastosphere for the slowly creeping lower layer; these terms are adopted in the following discussion.

Microstructural evidence for short-term deformation at extraordinary high stresses and strain rates of the uppermost plastosphere related to failure of the schizosphere (Scholz, 1990) in major seismic events in the geologic past has been reported from the Sesia Zone, Western Alps (Küster and Stöckhert, 1999). In a subsequent study, mechanical twinning of jadeite in metagranite was used as a paleopiezometer (Trepmann and Stöckhert, 2001), indicating that peak differential stresses probably exceeded 0.5 GPa. In some eclogitic micaschists, crystals of the high-strength mineral phase garnet embedded in a quartz and mica matrix are intensely fragmented. Their microstructures are markedly different from those of fragmented garnet described elsewhere (e.g. Valentino and Sclar, 1981; Prior, 1993; Wendt et al., 1993; Whitney, 1996; Ji et al. 1997; Whitney et al., 2000). Here we present a microstructural analysis of these fragmented garnet crystals and discuss the implications of the microstructural record for the processes of synseismic loading, postseismic creep and related changes of pore fluid pressure in the uppermost plastosphere.

2. Geological setting and description of specimens

The Sesia Zone in the Western Alps is derived from the basement of the southern overriding continent of the Alpine

* Corresponding author. Tel.: +49-234-3223235; fax: +49-234-3214572.

E-mail addresses: claudia.a.trepmann@ruhr-uni-bochum.de (C.A. Trepmann), bernhard.stoeckhert@ruhr-uni-bochum.de (B. Stöckhert).

[1] Tel.: +49-234-3223227/3227254.

0191-8141/02/$ - see front matter
PII: S0191-8141(02)00004-4

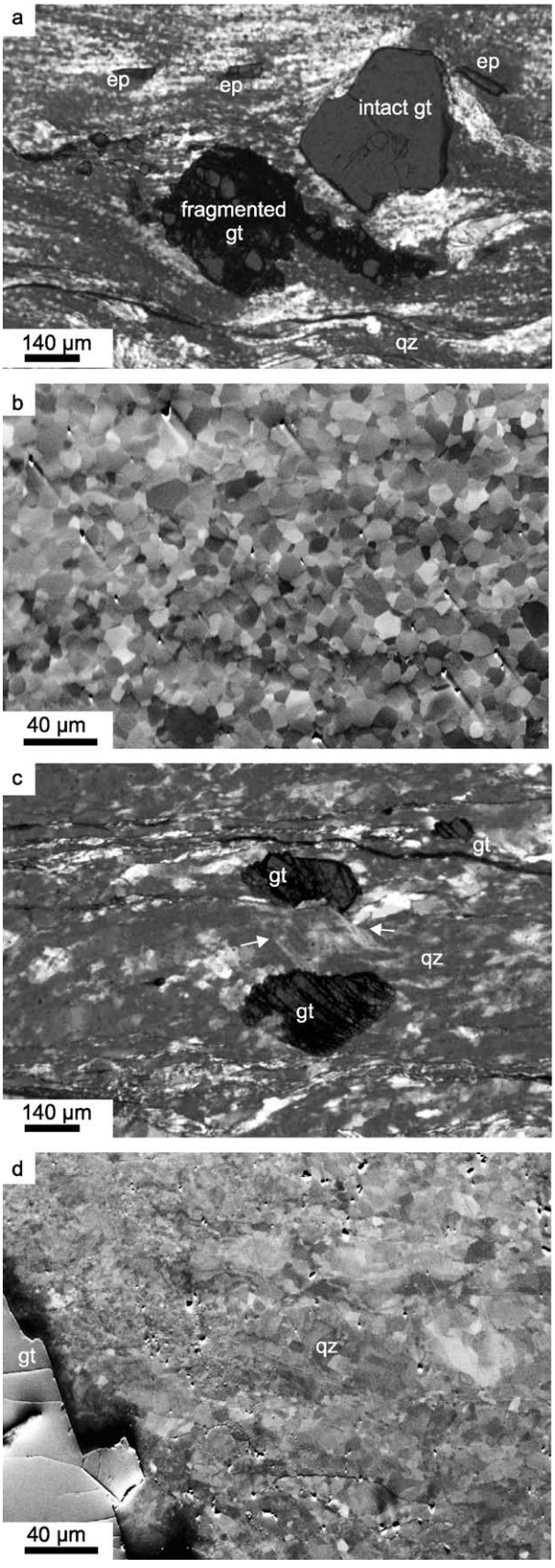

collision zone (Compagnoni et al., 1977). The rocks underwent an amphibolite to granulite facies metamorphism during Variscan times. During Alpine subduction and collision they were buried to about 60 km depth and underwent an eclogite facies high pressure metamorphism at $T = 550 \pm 50\,^{\circ}C$ and $P = 1.8 \pm 0.3$ GPa (Compagnoni, 1977; Pognante, 1989) in the late Cretaceous (Stöckhert et al., 1986; Inger et al., 1996).

In the lower Aosta valley of the Sesia Zone, the structures and microstructures developed during high pressure metamorphism are overprinted by a late stage inhomogeneous ductile deformation (Richter, 1984) at temperatures of about 300–350 °C (Stöckhert et al., 1986) and very high stresses. There, cataclastic flow of garnet has been reported from mylonitized eclogitic micaschists (Küster and Stöckhert, 1999).

Two specimens of mylonitic micaschist were chosen for analysis in this study (sample CT183: 409. 416 E, 5043. 518 N; sample St12: 409. 555 E, 5043. 528 N), each with a slightly different microstructural record of fragmented garnet. The main mineralogical constituents of both rocks are quartz (40–50%), phengite (30–40%) and garnet (10–15%), with minor K-feldspar, albite, omphacite, epidote, apatite, rutile and titanite. Petrographic descriptions of eclogitic micaschists of the lower Aosta Valley are found in Compagnoni (1977), Richter (1984) and Venturini (1995). Specimen St12 is from a high strain mylonite zone and shows a prominent foliation and lineation, while specimen CT183 is less deformed with no conspicuous lineation. The quartz matrix of the mylonite specimen St12 reveals pervasive dynamic recrystallization with a grain size down to about 5 μm (Fig. 1a and b), isometric grain shape and plane or curved grain boundaries, indicating that grain growth has affected the microstructure (Fig. 1b). In contrast, specimen CT183 shows a highly heterogeneous quartz microstructure (Fig. 1c and d) with marked gradients in the recrystallized grain size, that can be well below 5 μm at sites of stress concentration, but with larger grains preserved elsewhere which display prominent undulose extinction and locally abundant deformation lamellae.

3. Sample preparation and analytical techniques

The rock specimens were cut normal to the foliation and parallel to the lineation. Microstructural characteristics were analyzed from thin sections with an optical microscope. The

Fig. 1. (a) Optical micrograph showing one fragmented and one intact garnet embedded in a quartz matrix, mylonite specimen St12, crossed polarizers and Red I compensator inserted. Small particles in the quartz matrix are epidote. (b) OC-image of fine-grained quartz matrix, mylonite specimen St12. (c) Optical micrograph showing fragmented garnets embedded in a quartz matrix, with deformation lamellae parallel to fractures in garnet (arrows), specimen CT183, crossed polarizers and Red I compensator. (d) OC-image of the inhomogeneous quartz microstructure of specimen CT183.

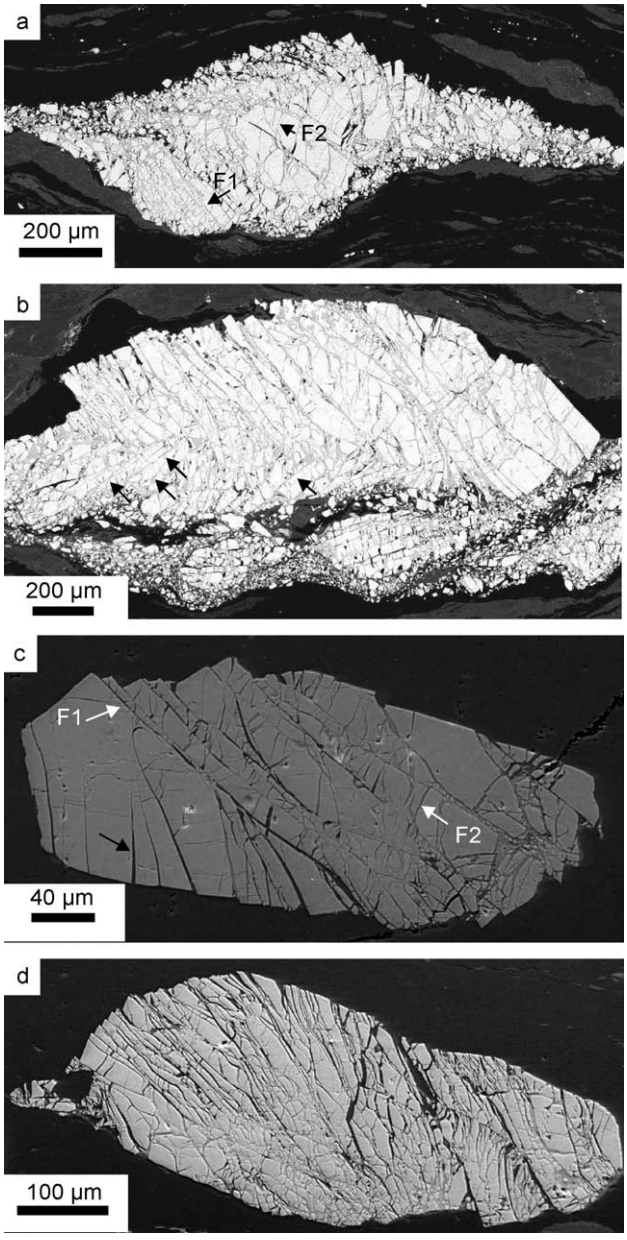

Fig. 2. (a) SE-image of cataclastic garnet with F1 and F2 fractures, mylonite specimen St12. (b) SE-image of cataclastic garnet with a second set of F1 fracture (arrows), mylonite specimen St12. (c) SE-image of cataclastic garnet showing F1 and F2 fractures (white arrows) and fractures oriented at a low angle to the shortening direction, terminating inside the grain (black arrow), specimen CT183. (d) SE-images of cataclastic garnet in specimen CT183.

orientation of the fracture planes in garnet was determined using a Leitz universal stage mounted on a Leitz Orthoplan microscope. For application of scanning electron microscopy (SEM), electron backscatter diffraction (EBSD) and orientation contrast (OC) techniques, the thin sections were chemically polished using a colloidal silicon suspension (SYTON®) to reduce the surface damage and coated with carbon to prevent charging effects. The chemical composition and zoning pattern of garnet was analyzed using an SX 50 electron microprobe from CAMECA. For element distribution mapping a CAMEBAX microprobe from CAMECA was used. Orientation and fine-scale structure—using the secondary electron (SE) signal—of the fractures in garnet were studied with a scanning electron microscope (SEM: LEO 1530; with field emission gun, forescatter detector, EBSD, and energy dispersive analytical facilities).

EBSD and OC-imaging are SEM-based methods for analyzing the crystallographic orientation of crystals in a thin section by using a backscattered electron (BSE) signal (e.g. Lloyd, 1987; Prior et al., 1996, 1999). The OC-method images the qualitative crystallographic misorientation between adjacent grains by grayscale contrast, although this does not correlate with the magnitude of misorientation. In contrast, EBSD analysis yields the full crystallographic orientation at a single spot. EBSD mapping was used to visualize the crystallographic orientation pattern for a selected area. In this case the specimen was moved automatically in a gridwise fashion underneath the focused electron beam and the crystallographic orientation was determined at each point. The crystallographic misorientation between two points is given by the lowest misorientation angle and the related rotation axis (Wheeler et al., 2001). This can be calculated from measurements on pairs of neighbor grains or for randomly selected pairs. For these methods the SEM was operated at an accelerating voltage of 25 kV, with the thin section tilted at an angle of 70° with respect to the beam, and with a working distance of 25 mm. The EBSD patterns were indexed with the software 'CHANNEL 4' (Schmidt and Olesen, 1989), that was also used for the presentation of the results of automatic orientation mapping. The automatic EBSD-maps are presented here without further processing, except for removing isolated points that were incorrectly indexed. For further processing of manual EBSD measurements, and for calculating misorientation axes, the computer program StereoNett 2.0 (Duyster, 1996) was used. For small misorientation angles, errors are large; therefore, misorientation axes for angles of less than 3° are neglected. The dispersion axis is defined as the maximum density of the orientation distribution of the misorientation axes. All stereographic diagrams are lower hemisphere projections.

4. Garnet microstructure

The microstructural characteristics of garnet in the two investigated specimens (St12, CT183) are described in the following paragraphs. In both specimens, the garnet crystals are embedded in a quartz and mica matrix (Figs. 1a and c and 2a–d). The majority (80–90%) of the garnet crystals show intense fragmentation, although a few crystals remain intact (Fig. 1a).

Two sets of microcracks are typically found in the fragmented garnet crystals. The first set, referred to as F1, is made up of pervasive plane or slightly curved transgranular

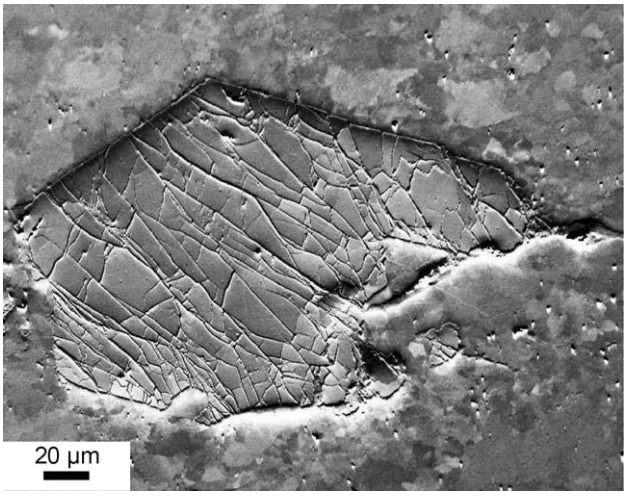

Fig. 3. OC-image of a fragmented garnet in specimen CT183, showing no displacement parallel to the fracture planes.

(Kranz, 1983) cracks (Fig. 2a–d). The orientation of F1 cracks is oblique to foliation and the direction of maximum shortening (Fig. 2a–d). In rare cases, fractures oriented almost perpendicular to foliation terminate within the grain (Fig. 2c). The second set of microcracks, referred to as F2, is made up of shorter fractures oriented at a high angle to the F1 fractures and abutting against them (Fig. 2a–d). This indicates that the F2 fractures developed after the F1 fractures. Typically, the fragments are displaced by a few micrometers predominantly along the F1 fractures (Figs. 1a and c and 2a–d). Notably, a few intensely cracked garnet crystals remain undistorted (Fig. 3).

The microcracks are generally restricted to the garnet crystals and a propagation into the surrounding matrix is not evident. In places, transgranular F1 fractures appear to be continuous with shear bands, revealing an apparent offset (possibly healed cracks), or deformation lamellae in the adjacent quartz matrix (Fig. 1c).

Electron microprobe data reveal a concentric and partly oscillatory zoning (Fig. 4a–c) of garnet with compositions in the range of almandine 73–50%, grossular 35–17%, pyrope 8–4%, spessartine 4–3%. Within the limits of spatial resolution, the chemical composition is not modified along the fractures, indicating that chemical reactions did not occur during or after fragmentation (Fig. 4a–c). Inclusions of apatite, ilmenite, mica, K-feldspar, and quartz in garnet are rare. There appears to be no correlation between fragmentation and garnet composition or the presence of inclusions.

4.1. Fracture pattern and geometry of fragmented garnet

The geometric characteristics of fragmented and deformed garnet in specimen CT183 are described by the following parameters (Fig. 5), determined by optical microscopy:

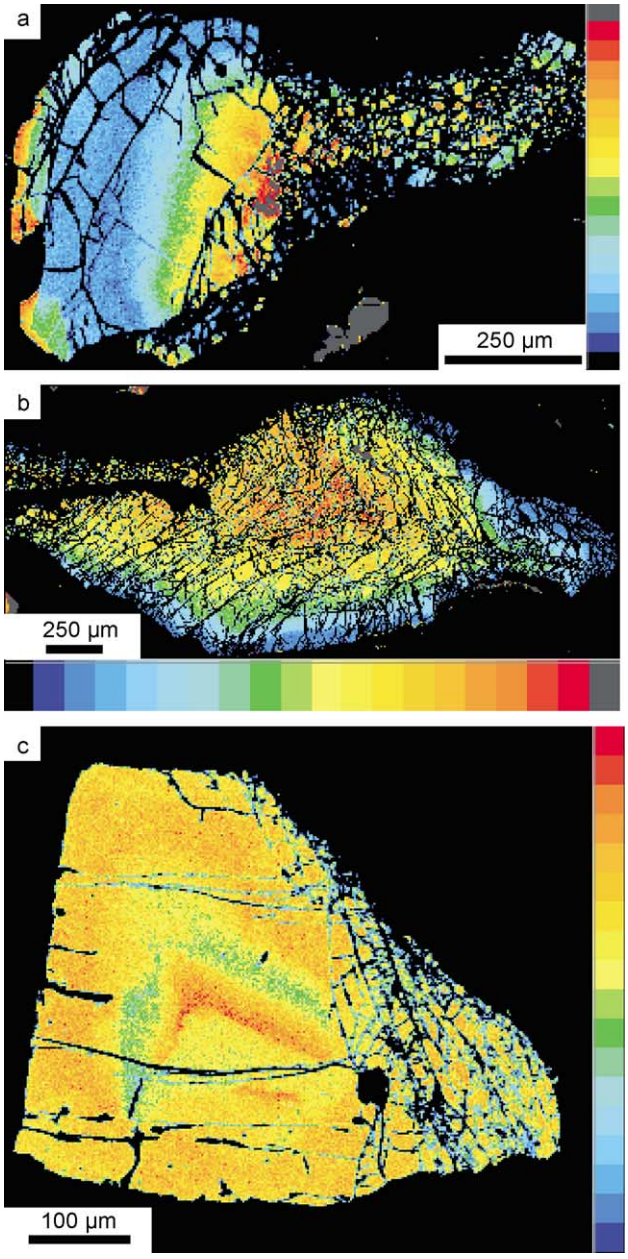

Fig. 4. Element distribution patterns (Calcium) of fragmented garnet. (a) Partly fragmented garnet in mylonite specimen St12. (b) Concentrical compositional zoning of a cataclastic garnet in mylonite specimen St12. (c) Oscillatory compositional zoning of a partly fragmented garnet in specimen CT183.

1. The long axis ($2L$), corresponding to the maximum diameter of the garnet;
2. The short axis ($2r$), corresponding to the maximum diameter of the garnet normal to the long axis;
3. The angle (β) between the long axis of the garnet and the foliation beyond the local perturbation caused by the garnet;
4. The orientation of F1 microcracks, described by the mean angle (α) between the fracture plane and the short axis of the garnet;

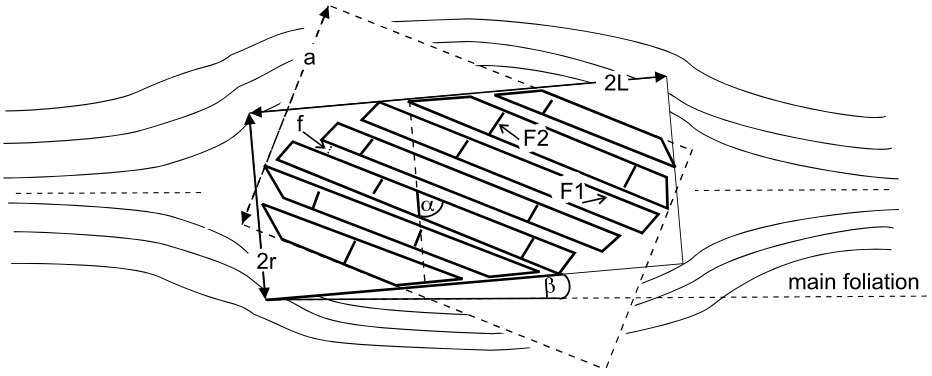

Fig. 5. Scheme showing the principal geometry of the fragmented garnets and the notation used in this study (see text for discussion).

5. The fracture density (n/a), measured as the number of F1 fractures normalized to the length $a$perpendicular to the F1 fracture;
6. The typical width of opening of the cracks (f), measured normal to the crack.

From these parameters the aspect ratio s, the grain size d, and the distance a (Fig. 5) were calculated as follows:

$$s = L/r \quad (1)$$

$$d = 2(Lr)^{1/2} \quad (2)$$

$$a = 2L\cos(\alpha) \quad (3)$$

The grain size of garnet ranges from 0.2 to 2.4 mm (average 0.8 mm) and shows no correlation with density of F1 fractures n/a (Fig. 6a). Fragmented garnets show a relatively high aspect ratio ($s = 2.0$, on average, with extremes of 1.0 and 3.5; Fig. 6b). In contrast, intact garnets reveal a low aspect ratio of 1.3 on average. The angle β between the long axis of the fragmented garnets and the foliation is typically between 0 and 20°. The angle α (Fig. 5) is 42° on average, with extremes of 10 and 72° (Fig. 6c). There appears to be neither a correlation between the fracture density n/a and the grain size, nor to the aspect ratio or to the angle α (Fig. 6a–c). However, stereological effects cannot be ruled out, as small garnets with high fracture densities may represent near-rim sections through larger garnets.

The fracture-normal displacement along dilatant fractures (f) is about 1.5 μm on average, with extremes of 0.2 and 5 μm (Figs. 2a–d and 7b), as seen in the SEM. These opened cracks are filled with quartz and feldspar. In general dilation is small and uniform (cf. Figs. 2c and d, 3 and 7d) and the fragments reveal a high degree of fitting.

In contrast to specimen CT183, the garnet fragments in the high strain mylonite St12 are widely separated and have undergone significant rotation, where they form continuous thin layers or streaks parallel to the mylonitic foliation (cf. Figs. 2a and b and 4a and b). In some of these garnets the F1 fractures form a conjugate system with angles α between 20 and 70°, and between 100 and 170°, respectively. Some large garnets show two sets of F1 fractures at an angle of about 90° (cf. Figs. 2b, 4b, 7a and 8c).

4.2. Crystallographic orientation

The crystallographic orientation of fragmented and disintegrated garnet was studied to examine rotation of fragments during deformation, crystallographic control on crack orientation, the influence of preexisting low angle grain boundaries (LAGB) on fracture location, and potential effects of crystallographic orientation on brittle strength.

First, the OC-images (Figs. 3 and 7b) show that a crystallographic misorientation between the individual fragments is common for the fragmented garnets, while the crystallographic orientation is rather uniform within an individual fragment. In a detailed inspection, the crystallographic orientation of 63 garnets of specimen CT183 and 10 garnets of the mylonite specimen St12 were analyzed with the EBSD-technique.

The crystallographic misorientation between neighboring fragments is typically between 5 and 10°, as shown by the relative frequency of neighbor-pair misorientation angles (Fig. 8a–c). However misorientations of up to 30° were found in specimen CT183 and of up to 40° in the mylonite specimen St12. Some of the higher values obtained by the automatic measurements may be due to misindexing. The misorientation profile in Fig. 8b shows that the magnitude of cumulative misorientation increases progressively across the disintegrated grain. Most non-neighbor, randomly selected pairs from garnets in specimen CT183 reveal misorientations of typically 10–15° (Fig. 8a and b). In contrast, the relative frequency of misorientation angles of randomly selected pairs from large garnets in the mylonite specimen St12, with two sets of F1 fractures (Figs. 2b, 4b and 7a), reveals a maximum at about 45–50° (Fig. 8c). The contrast between the random-pair and the neighbor-pair misorientation distribution, which can be quantified by the Kolmogorov–Smirnov test (Wheeler et al., 2001) is

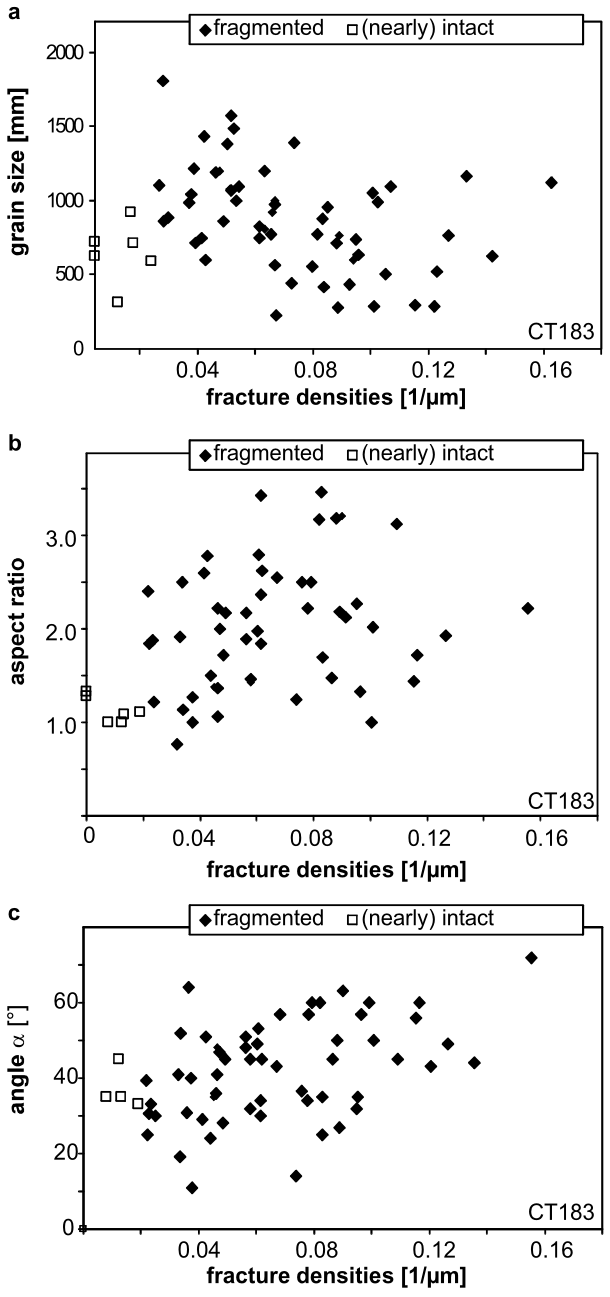

Fig. 6. (a) Plot of the grain size of garnet versus F1 fracture density (n/a) (specimen CT183). (b) Plot of the aspect ratio of garnet versus F1 fracture density (n/a) (specimen CT183). (c) Plot of the angle α versus F1 fracture density (n/a) (specimen CT183).

visualized in Fig. 9. This shows that the highest degree of fragmentation and disintegration (Fig. 8c, compare Fig. 4b) correlates with the largest difference between the two misorientation distributions.

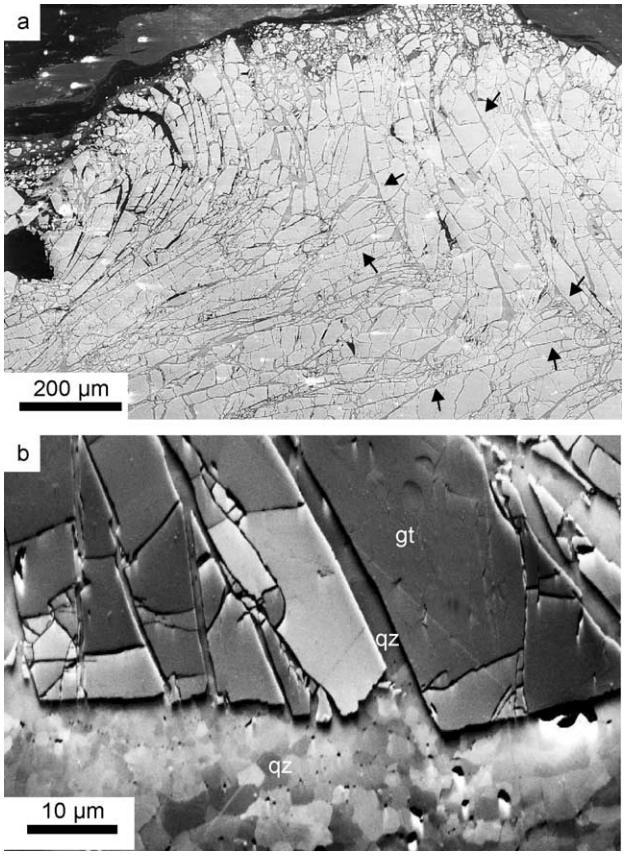

Fig. 7. (a) SE-image of a fragmented garnet in mylonite specimen St12, revealing two domains with F1 fractures at a high angle to each other (arrows). (b) OC-image of fragmented garnet in specimen CT183; open cracks are sealed with quartz and feldspar.

In 65% of the investigated cases the crystallographic orientations of the fragments are dispersed around one axis, as shown in the stereographic plots (Figs. 8b and c and 10). This dispersion axis is defined by the maximum density of the orientation distribution of the misorientation axes (Fig. 10c). Furthermore, for nearly 50% of the investigated cases the dispersion axis plots within a few degrees of a crystallographic axis: 25% near to ⟨100⟩ (e.g. Fig. 10b); 12% near to ⟨110⟩ and 12% near to ⟨111⟩. In contrast, the angle between the dispersion axis and the normal to the fracture plane varies from 14 to 90° and averages 63°.

The fractures do not follow rational planes, as can be seen by comparing the crystallographic orientation of the garnet fragments and the orientation of the F1 fracture plane (example in Fig. 10), measured with the universal stage on the optical microscope. In only 25% of the investigated cases the normals to the fracture planes are oriented near a crystallographic axis. In view of the high symmetry of

Fig. 8. (a) EBSD-map of fragmented and slightly disintegrated garnet in specimen CT183 (compare Fig. 2c). Right: Histogram of the relative frequency of misorientation angles and stereographic plot of the crystallographic planes. (b) EBSD-map of fragmented and disintegrated garnet in mylonite specimen CT183. Bottom: Misorientation profile along the line in the EBSD-map. Right: histogram of the relative frequency of misorientation angles and stereographic plot of the crystallographic planes. (c) EBSD-map of fragmented and strongly disintegrated garnet in mylonite specimen St12 (compare Fig. 4b). Right: Histogram of the relative frequency of misorientation angles and stereographic plot of the crystallographic planes.

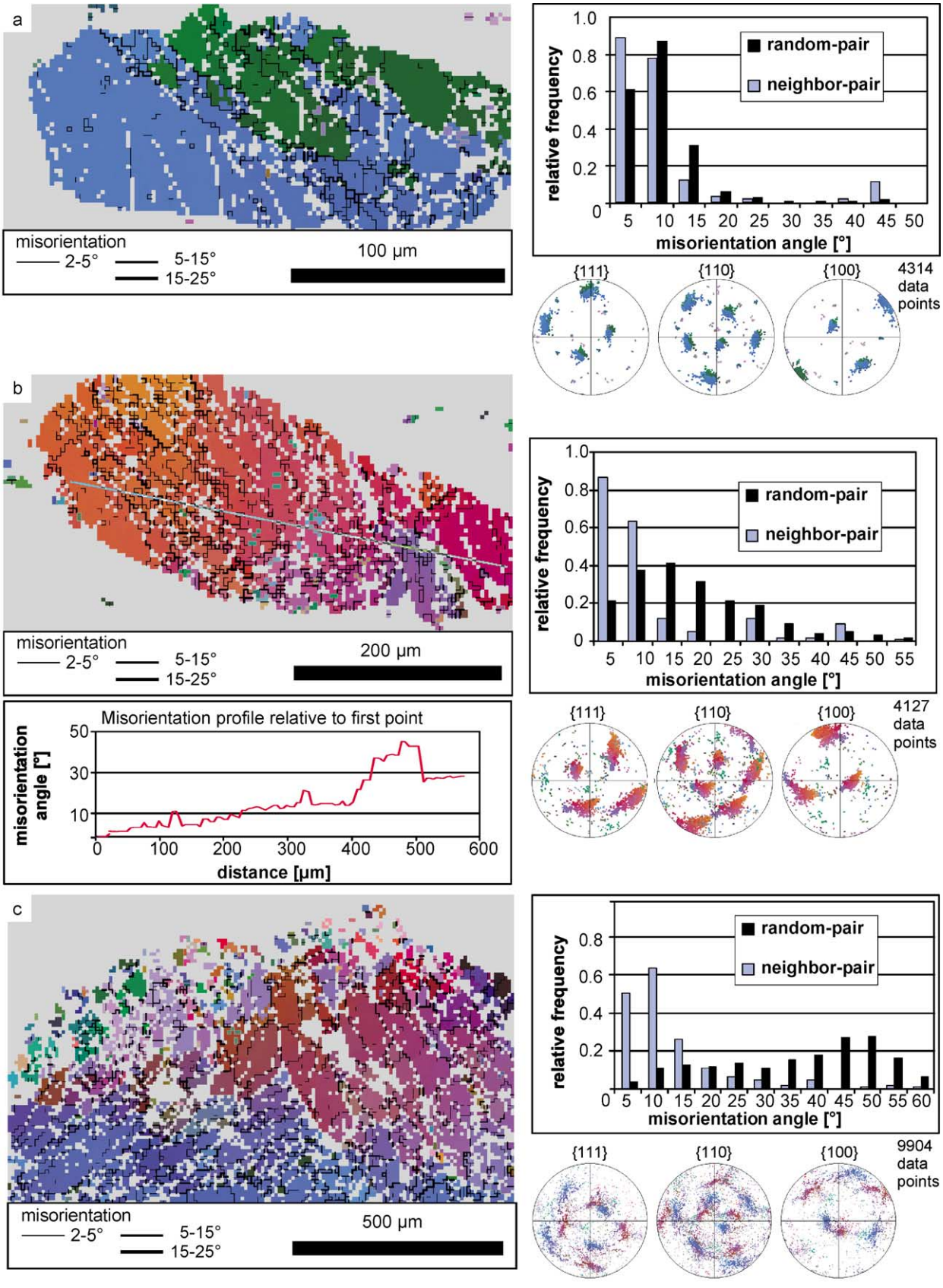
a
misorientation
2-5°
5-15°
15-25°
100 µm
relative frequency
random-pair
neighbor-pair
misorientation angle [°]
{111}
{110}
{100}
4314 data points
b
misorientation
2-5°
5-15°
15-25°
200 µm
relative frequency
random-pair
neighbor-pair
misorientation angle [°]
{111}
{110}
{100}
4127 data points
Misorientation profile relative to first point
misorientation angle [°]
distance [µm]
c
misorientation
2-5°
5-15°
15-25°
500 µm
relative frequency
random-pair
neighbor-pair
misorientation angle [°]
{111}
{110}
{100}
9904 data points

garnet, this can be assumed to occur by chance. Also, no direct effect of a specific crystallographic orientation on the degree of fragmentation and disintegration was observed.

Some undeformed garnet crystals display low angle grain boundaries (LAGB) with a small misorientation of $<3°$ (Fig. 11a and c). In a partly fragmented garnet crystal (Fig. 11a), a LAGB with a misorientation angle of $<2°$ grades into a microcrack with a crystallographic misorientation of up to 14°. The rotation axis for the misorientation across the LAGB is inclined to the fracture normal with an angle of about 60°, whereas the rotation axis for the crystallographic misorientation along the fracture is oriented at an angle of 85–89°, suggesting a twist geometry of displacement. There is no relation between the compositional zoning of the garnet and the domains of different crystallographic orientations (compare Figs. 4c and 11a).

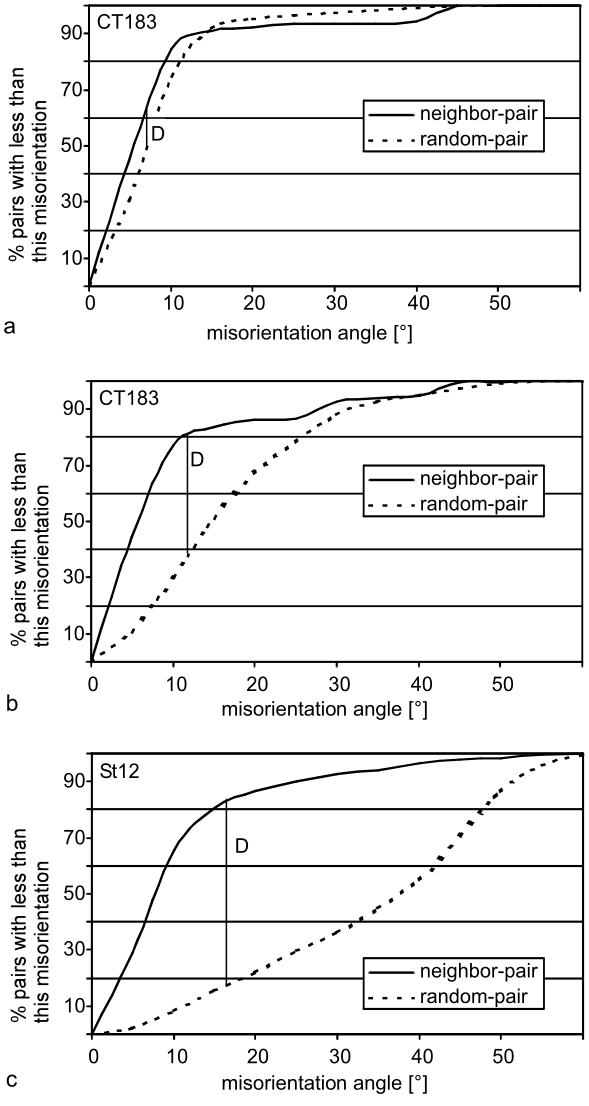

Fig. 9. Cumulative frequency diagrams showing neighbor-pair and random-pair misorientation distribution and illustrating the Kolomogrov–Smirnov test for significant differences (Wheeler et al., 2001). (a) Lowest difference *D* in misorientation distribution in slightly disintegrated garnet from specimen CT183 (compare EBSD-map, Fig. 8a). (b) Difference *D* in misorientation distribution in moderately disintegrated garnet from specimen CT183 (compare EBSD-map, Fig. 8b). (c) Highest difference *D* in misorientation distribution in strongly disintegrated garnet from specimen ST12 (compare EBSD-map, Fig. 8c).

5. Discussion

5.1. Implications of the microstructural record

Both intact garnet crystals and fragmented garnet that remained undistorted (Fig. 3) show a low aspect ratio. This indicates that the high aspect ratio of the distorted garnet was caused by frictional sliding along cracks. Fragmentation appears not to be restricted to crystals with a specific aspect ratio or to any evident local matrix property. Furthermore, fragmented garnet crystals that remained undistorted (Fig. 3) show that fragmentation was not necessarily followed by translation of the fragments along the cracks. Thus, the displacement along the fracture plane is not directly related to the initial stage of fragmentation. This is consistent with the rather uniform displacement along the cracks, as seen in Figs. 2a–d, 3 and 10a, indicating that the

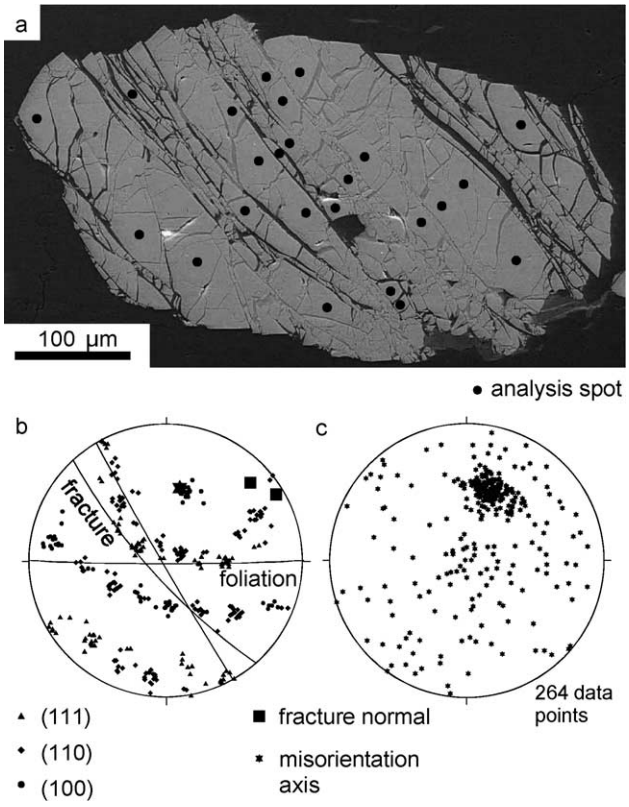

Fig. 10. (a) SE-image of a fragmented garnet with sites of manual EBSD measurements. (b) Stereographic plot of the fracture planes, misorientation axes and crystallographic orientation of the garnet in (a). (c) Stereographic plot of misorientation axes (calculated from EBSD measurements with the computer program StereoNett 2.0; Duyster, 1996), with the maximum density defining the dispersion axis.

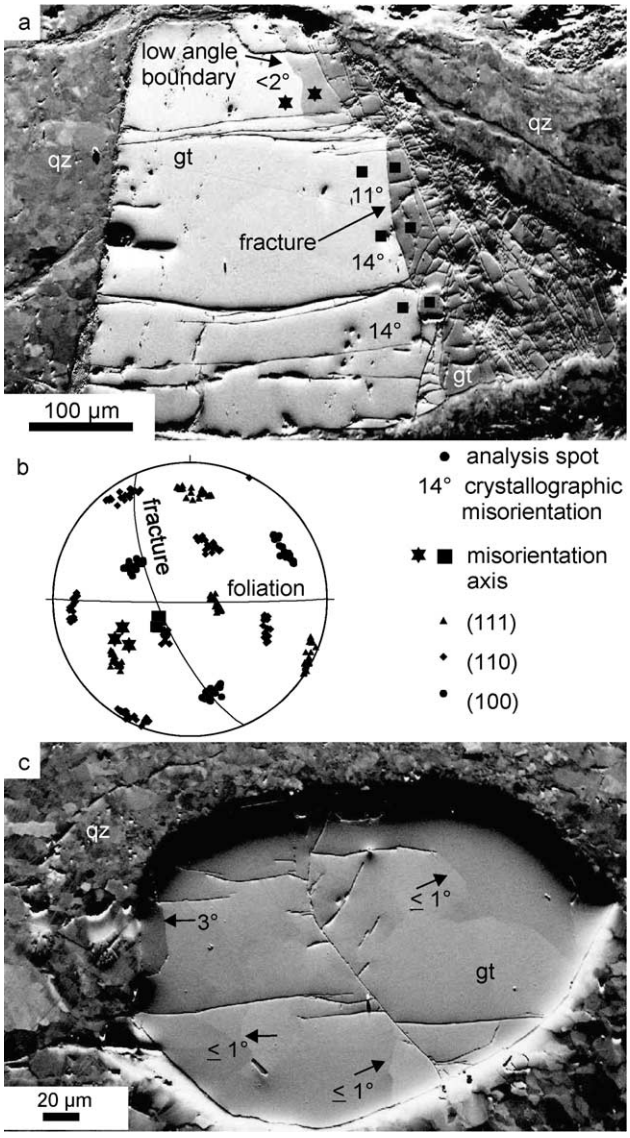

Fig. 11. (a) OC-image of a partly fragmented garnet with sites of manual EBSD-measurement. The angle of misorientation along the low angle boundary and the fracture (arrows) is indicated. (b) Stereographic plot of the crystallographic orientation, the misorientation axes and the fracture plane of the garnet in (a). (c) OC-image of an intact garnet crystal with low angle grain boundaries (arrows) and corresponding angle of misorientation.

cracks already existed when translation by frictional sliding took place.

As intact garnet crystals and individual fragments show no, or only very small, internal variation in crystallographic orientation of $<3°$ (Fig. 11a and c), the observed misorientation between the fragments is likely to have developed after fracturing of an original single crystal with at best only a few low angle grain boundaries. The progressive increase of the magnitude of cumulative misorientation across a disintegrated grain (Fig. 8b) and the positive correlation between the degree of disintegration and the contrast between random-pair and neighbor-pair misorientation distributions (Figs. 8 and 9), suggest that the high misorientations are due to rotation of the fragments. The dispersion axes (Figs. 8b and c and 10) are inclined with an angle of 14–90° to the fracture plane, indicating partly complex displacement paths. The domainal orientation distribution of F1 fractures observed in some of the larger garnets (Figs. 2b, 4b, 7a and 8c) is interpreted to be the result of buckling (Fig. 12), supported by the untypically large maximum misorientation of 45–50° between non-neighboring fragments (Fig. 7b).

The observation of LAGB's in intact garnets and within large fragments (Fig. 11a and b), suggests that some of the fractures may have followed preexisting LAGB's. Garnet substructures with a crystallographic misorientation of $<3°$ were attributed to deformation by dislocation creep by Prior et al. (2000). However, formation of LAGB's as growth irregularities or during growth of porphyroblasts by agglomeration (Spiess et al., 2001) cannot be ruled out. The compositional maps, however, show no evidence for development by multiple nucleation, as concentric growth zoning is dominant and is even still discernible in some strongly fragmented and distorted garnets (Figs. 4b and 8c).

5.2. Conditions at initial fragmentation

Brittle failure of stiff inclusions in a ductile matrix depends on the stress transfer from the matrix to the inclusion (e.g. Boullier, 1980; White et al., 1980). One of the favored theoretical models is the fiber loading mechanism (e.g. Ji and Zhao, 1994; Zhao and Ji, 1997), which has been applied to the development of tensile fractures in garnet in anisotropic metamorphic rocks during exhumation (Ji et al., 1997). Their model shows that the garnets become disintegrated through progressive mid-point fracturing, with cracks at right angles to the long axis of the inclusion. This model can explain the formation of sets of parallel, straight, fractures at a low angle to the maximum principal stress direction. However, progressive mid-point fracturing in a slowly creeping matrix is difficult to reconcile with the microstructural record of garnet described in this study. First, it would be expected that displacement along the cracks should reflect the relative age of the fractures, with larger displacements along the earlier generations. As seen in Figs. 2a–d, 3 and 10a both the fracture-parallel displacement and the fracture-normal displacement in the case of opened cracks is rather uniform, indicating a similar age of the cracks and a common subsequent history. Second, given the small size of the fragments, the preservation of large intact garnet crystals nearby would probably require an extremely heterogeneous stress field, if progressive mid-point fracturing in a flowing matrix is assumed.

Multiple tensile, shear, and extensional shear fracturing of stiff inclusions hosted in a ductile matrix was addressed in experiments and modeled by Mandal et al. (2001). These authors show that the aspect ratio and the orientation of the inclusions control the internal principal tensile and compressive stresses and, thus, control the mode of failure.

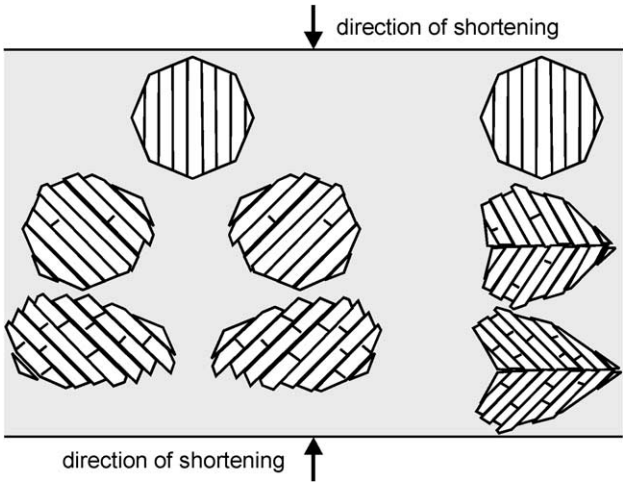

Fig. 12. Scheme visualizing the inferred progressive cataclastic deformation of garnet crystals, planes and buckling of fragments (see text).

They also found that the stress inside an inclusion is homogenous and that the magnitude of the maximum principal compressive stress is inversely proportional to the ellipticity of the inclusion, so that shear fracturing is favored for a low aspect ratio. At a given confining pressure and bulk strain rate inclusions with an axial ratio below a critical value do not fracture at all and remain intact.

Following the results of Mandal et al. (2001), the original low aspect ratio of the garnets in our study would suggest failure by shear fractures. However, the F1 fracture sets in garnet of specimen CT183 show a uniform inclination to the foliation, even in undistorted garnet (Fig. 3). Furthermore, conjugate crack systems are not observed, as would be expected for shear fracture. In the highly distorted garnet of the mylonite specimen St12 the apparent conjugate systems observed could have developed during rotation by progressive deformation (Fig. 12), with coalescence of F2 cracks. If fragmentation was by formation of tensile cracks, with the fracture planes oriented parallel to the maximum principal stress σ_1 direction, the orientation of σ_1 at the instant of crack formation could have been oblique to the foliation, or the cracks may have been reoriented by uniform rotation of the fragments in simple shear.

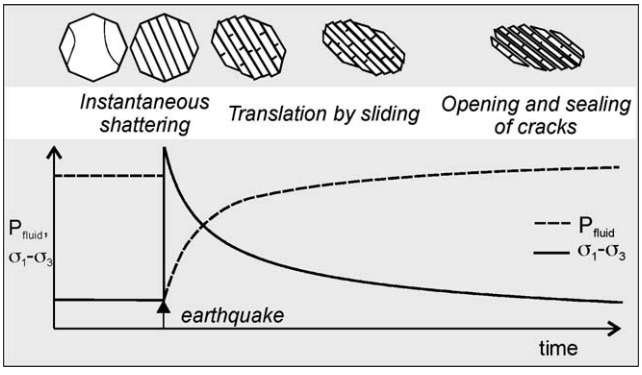

Fig. 13. Proposed model relating cataclastic deformation of garnet to synseismic loading and postseismic creep (see text for discussion).

Shear bands and sets of deformation lamellae in the quartz matrix that parallel the fractures in garnet (Fig. 1c) may represent healed cracks. A correlation of these features with either the stage of garnet fragmentation or that of subsequent displacement is not possible, as the microstructural record is obliterated due to plastic flow and recrystallization of the quartz matrix. However, a pervasive cataclastic disintegration of the rock cannot be ruled out.

Despite the uncertainty regarding the mode of formation of the F1 fractures, we propose a quasi-instantaneous fragmentation, with all F1 cracks formed nearly simultaneously, followed by distortion of the aggregate in the creeping quartz matrix. A well-defined yield stress for the fragmentation of the garnet is probably the reason why some crystals remained intact at sites where the critical value was not attained due to minor heterogeneities in the stress field.

5.3. Tectonic environment and inferred boundary conditions

Garnet is a high strength mineral phase, well-known through its occasional use as an abrasive. For non-silicon garnet, brittle strength has been investigated in material science using microindentation and fracturing techniques. These experiments suggest a very high theoretical cohesive strength (extensional) of 49 GPa, which is comparable with that of corundum (e.g. Pardavi-Horváth, 1984; Reimanis et al., 1994). Thus, brittle deformation of natural garnet is expected to be restricted to extraordinary conditions with very high stresses and strain rates. For instance, Austrheim and Boundy (1994) and Austrheim et al. (1996) attributed garnet fragmentation combined with the occurrence of pseudotachylites to seismic activity in the lower crust. Degenhardt et al. (1994) also describe localized cataclastic comminution of garnet in granite gneisses of the Roter Kamm impact crater, Namibia.

It has been proposed that the microstructural record of the rocks of the Sesia Zone described in this study was acquired when they had attained a position in the uppermost plastosphere, just beneath the brittle–plastic transition (Küster and Stöckhert 1999; Trepmann and Stöckhert, 2001), during a period of major seismic activity in the overlying schizosphere. In this case, instantaneous stress redistribution during major earthquakes causes synseismic loading and short term postseismic creep in the uppermost plastosphere, with a strain-rate dependent transient downward displacement of the brittle–plastic transition. Mechanical twinning of clinopyroxene indicates that the rocks were exposed to very high stresses (possibly >0.5 GPa; Trepmann and Stöckhert, 2001), implying near-laboratory strain rates and markedly sublithostatic pore fluid pressure (Küster and Stöckhert, 1999).

Quasi-instantaneous shattering of the garnet crystals—fragmentation by F1 cracks—is proposed to have taken place (Fig. 13) at the stage of synseismic loading.

Subsequently, during decay of the synseismically created stresses, the fragments were displaced by frictional sliding along the fractures (Fig. 13). At this stage, deformation of garnet was controlled by rapidly decelerating dislocation creep in the surrounding quartz matrix.

The very high stresses in the early stage of fragmentation are not compatible with a notable pore fluid pressure. Therefore the rocks must have been either essentially dry, which appears unlikely in view of the fluid inclusions along healed cracks described by Küster and Stöckhert (1999), or the pore fluid pressure has dropped due to dilatation and a transient high permeability related to fractures synseismically propagating down to depth where deformation usually processes by slow and pressure-insensitive fully plastic creep. The opening of the cracks in garnet at a very late stage of deformation, with open space being filled by quartz and feldspar precipitated from the pore fluid (Fig. 13), suggests that the pore fluid pressure regained a near-lithostatic value in the final stage of postseismic creep. Little strain has been accumulated at this late stage, as shown by the small crack-normal displacement, while fracture-parallel sliding had dominated during the major part of postseismic creep.

6. Conclusions

The microstructural record of fragmented garnet corresponds to the previously proposed interpretation of the peculiar late stage and moderate temperature microstructural record of high pressure metamorphic rocks of the Sesia Zone, Western Alps (Küster and Stöckhert, 1999; Trepmann and Stöckhert, 2001). Also, it is consistent with the processes of synseismic loading, related to major seismic activity in the overlying schizosphere, and stress relaxation combined with reconstitution of a near-lithostatic pore fluid pressure during postseismic creep of the uppermost plastosphere, reconciling with an earthquake cycle. It should be noted, however, that unequivocal evidence for multiple loading and creep stages has not yet been identified.

The inferred microstructural evolution of garnet, schematically depicted in Fig. 13, can thus be subdivided into three stages:

1. Quasi-instantaneous shattering of the garnet crystals during synseismic loading to high peak-stresses, with pore fluid pressure dropping to markedly sub-lithostatic values, preventing an opening and sealing of the microcracks.
2. Progressive displacement of the garnet fragments by frictional sliding along the fractures, controlled by rapidly decelerating dislocation creep in the surrounding quartz matrix, reflecting the main stage of postseismic creep and stress relaxation.
3. Late stage deformation driven by residual stresses, with garnet fragments becoming separated by a crack-normal component of displacement. At this stage pore fluid pressure must have attained near-lithostatic values, permitting opening of the cracks and sealing by quartz and feldspar precipitated from the pore fluid. The strain accumulated at this final stage of postseismic creep is small.

Clearly, fundamental questions concerning the load transfer between a weak matrix and a stiff inclusion, and the mode of failure at the stage of fragmentation, are unresolved and deserve further consideration. Nevertheless, we feel that the microstructural record of exhumed, mid-crustal rocks can provide valuable insight into processes and boundary conditions relevant to present-day earthquakes.

Acknowledgements

Rolf Neuser is thanked for support at the SEM, Johannes Duyster for advice with the OC and EBSD-techniques, and Stuart Thomson for kindly improving the English. Funding by the German Science Foundation within the scope of the Collaborative Research Center 526 "Rheology of the Earth—from the upper crust into the subduction Zone" is gratefully acknowledged. Shaocheng Ji and David Prior are thanked for the constructive reviews.

References

Austrheim, H., Boundy, T.M., 1994. Pseudotachylites generated during seismic faulting and eclogitization of the deep crust. Science 265, 82–83.

Austrheim, H., Erambert, M., Boundy, T.M., 1996. Garnets record in deep crustal earthquakes. Earth and Planetary Science Letters 193, 223;238.

Boullier, A.M., 1980. A preliminary study on the behaviour of brittle minerals in a ductile matrix: example of zircon and feldspars. Journal of Structural Geology 2, 211–217.

Brace, W.F., Kohlstedt, D.L., 1980. Limits on lithospheric stress imposed by laboratory experiments. Journal Geophysical Research 85, 6248–6252.

Compagnoni, R., 1977. The Sesia–Lanzo Zone: high pressure–low temperature metamorphism in the austroalpine continental margin. Rendiconti Societa Italiana della Mineralogia e Petrologia 33, 335–374.

Compagnoni, R., Dal Piaz, G.V., Hunziker, J.C., Gosso, G., Lombardo, B., Williams, P.F., 1977. The Sesia–Lanzo Zone, a slice of continental crust with alpine high pressure–low temperature assemblages in the western Italian Alps. Rendiconti Societa Italiana della Mineralogia e Petrologia 33, 281–334.

Degenhardt, J.J., Buchanan, P.C., Reid, A.M., Miller, R.McG., 1994. Breccia veins and dykes associated with Roter Kamm Crater, Namibia. Geological Society of America, Special Paper 293, 197–208.

Duyster, J., 1996. StereoNett 2.0, University of Bochum.

Evans, B., Kohlstedt, D.L., 1995. Rheology of rocks. In: Ahrens, T.J. (Ed.). Rock Physics and Phase Relations—A Handbook of Physical Constants. Ref. Shelf 3, Am. Geophys. Un., pp. 148–165.

Goetze, C., Evans, B., 1979. Stress and temperature in the bending lithosphere as constrained by experimental rock mechanics. Geophysical Journal of the Royal Astronomical Society 59, 463–478.

Inger, S., Ramsbotham, W., Cliff, R.A., Rex, D.C., 1996. Metamorphic evolution of the Sesia–Lanzo-Zone, Western Alps: time constraints

from multi-system geochronology. Contributions Mineralogy and Petrology 126, 152–168.

Ji, S., Zhao, P., 1994. Strength of two-phase rocks: a model based on fiber-loading theory. Journal of Structural Geology 16, 253–262.

Ji, S., Zhao, P., Saruwatari, K., 1997. Fracturing of garnet crystals in anisotropic metamorphic rocks during uplift. Journal of Structural Geology 19, 603–620.

Kohlstedt, D., Evans B., Mackwell, S.J., 1995. Strength of the lithosphere: Constraints imposed laboratory experiments. J. Geophys. Res. B9, 17587–17602.

Kranz, R.L., 1983. Microcracks in rocks: a review. Tectonophysics 100, 449–480.

Küster, M., Stöckhert, B., 1999. High differential stress and sublithostatic pore fluid pressure in the ductile regime—microstructural evidence for short term postseismic creep in the Sesia Zone, Western Alps. Tectonophysics 303, 263–277.

Lloyd, G.E., 1987. Atomic number and crystallographic contrast images with the SEM: a review of backscattered electron techniques. Mineralogical Magazine 51, 3–19.

Mandal, N., Chakraborty, C., Samanta, S.K., 2001. Controls on the failure mode of brittle inclusions hosted in a ductile matrix. Journal of Structural Geology 23, 51–66.

Pardavi-Horváth, M., 1984. Microhardness and brittle fracture of garnet single crystals. Journal of Materials Science 19, 1159–1170.

Pognante, U., 1989. Lawsonite, blueschist and eclogite formation in the southern Sesia Zone, western Alps, Italy. European Journal of Mineralogy 1, 89–104.

Prior, D.J., 1993. Sub-critical fracture and associated retrogression of garnet during mylonitic deformation. Contributions to Mineralogy and Petrology 113, 545–556.

Prior, D.J., Trimby, P.W., Weber, D.U., Dingley, D., 1996. Orientation contrast imaging of microstructures in rocks using forescatter detectors in the scanning electron microscope. Mineralogical Magazine 60, 859–869.

Prior, D.J., Wheeler, J., Brenker, F., Harte, B., Matthews, M., 2000. Crystal plasticity of natural garnet: new microstructural evidence. Geology 28, 1003–1006.

Prior, J.P., Bolyle, A.P., Brenker, F., Cheadle, M.C., Day, A., Lopez, G., Peruzzo, L., Potts, G.J., Reddy, S., Spiess, R., Timms, N.E., Trimby, P., Wheeler, J., Zetterström, L., 1999. The application of electron backscatter diffraction and orientation contrast imaging in the SEM to textural problems in rocks. American Mineralogist 84, 1741–1759.

Reimanis, I.E., Petrovic, J.J., Mitchell, T.E., 1994. The fracture behavior of single-crystal $Y_3Al_5O_{12}$. Journal of Non-Crystalline Solids 177, 67–73.

Richter, F., 1984. Deformation und Metamorphose in der alpinen SubduktionsZone: Die Sesia–Lanzo-Zone im unteren Val d'Aosta, Norditalien. Unpubl. Thesis University of Bonn.

Schmidt, N.H., Olesen, N., 1989. Computer-aided determination of crystal-lattice orientation from electron-channeling patterns in the SEM. Canadian Mineralogist 27, 15–22.

Scholz, C.H., 1990. The Mechanics of Earthquakes and Faulting. Cambridge University Press, Cambridge.

Sibson, R.H., 1980. Transient discontinuities in ductile shear zones. Journal of Structural Geology 2, 165–171.

Spiess, R., Peruzzo, L., Prior, D.J., Wheeler, J., 2001. Development of garnet porphyroblasts by multiple nucleation, coalescence and boundary misorientation driven rotations. Journal of Metamorphic Geology 19, 269–290.

Stöckhert, B., Jäger, E., Voll, G., 1986. K–Ar age determinations on phengites from the internal part of the Sesia Zone, Western Alps, Italy. Contributions to Mineralogy and Petrology 92, 456–470.

Trepmann, C., Stöckhert, B., 2001. Mechanical twinning of jadeite—an indication of synseismic loading beneath the brittle–ductile transition. International Journal of Earth Science 90, 4–13.

Valentino, A.J., Sclar, C.B., 1981. Parting in giant garnets as an indicator of late brittle deformation at Gore Mountain, Warren County, NY. Geophysical Research Letters 8, 883–885.

Venturini, G., 1995. Geology, geochemistry and geochronology of the inner central Sesia Zone, Western Alps, Italy. Mémoires de Géologie No. 25, Lausanne.

Wendt, A.S., D'Arco, P., Goffé, B., Oberhänsli, R., 1993. Radial cracks around a quartz inclusions in almandine: Constraints on the metamorphic history of the Oman mountains. Earth and Planetary Science Letters 114, 449–461.

Wheeler, J., Prior, D.J., Jiang, Z., Spiess, R., Trimby, P.W., 2001. The petrological significance of misorientations between grains. Contributions to Mineralogy and Petrology 141, 109–124.

White, S.H., Burrows, S.E., Carreras, J., Shaw, N.D., Humphreys, F.J., 1980. On mylonites in ductile shear Zones. Journal of Structural Geology 2, 175–187.

Whitney, D.L., 1996. Garnets as open systems during regional metamorphism. Geology 24, 147–150.

Whitney, D.L., Cooke, M.L., Du Frane, S.A., 2000. Modeling of radial microcracks at corners of inclusions in garnet using fracture mechanics. Journal of Geophysical Research 105, 2843–2853.

Yeats, R.S., Sieh, K., Allen, D.R., 1997. The Geology of Earthquakes. Oxford University Press, New York.

Zhao, P., Ji, S., 1997. Refinements of shear-lag model and its applications. Tectonophysics 279, 37–53.